



**HAL**  
open science

## Natural conditions for more limited osmotic abnormal fluid pressures in sedimentary basins

Joachim Tremosa, Julio Goncalves, Jean-Michel Matray

► **To cite this version:**

Joachim Tremosa, Julio Goncalves, Jean-Michel Matray. Natural conditions for more limited osmotic abnormal fluid pressures in sedimentary basins. *Water Resources Research*, 2012, 48, pp.W04530. 10.1029/2011WR010914 . hal-00833528

**HAL Id: hal-00833528**

**<https://hal.science/hal-00833528>**

Submitted on 1 Nov 2021

**HAL** is a multi-disciplinary open access archive for the deposit and dissemination of scientific research documents, whether they are published or not. The documents may come from teaching and research institutions in France or abroad, or from public or private research centers.

L'archive ouverte pluridisciplinaire **HAL**, est destinée au dépôt et à la diffusion de documents scientifiques de niveau recherche, publiés ou non, émanant des établissements d'enseignement et de recherche français ou étrangers, des laboratoires publics ou privés.

Copyright

## Natural conditions for more limited osmotic abnormal fluid pressures in sedimentary basins

Joachim Tremosa,<sup>1,2</sup> Julio Gonçalves,<sup>3</sup> and Jean-Michel Matray<sup>2</sup>

Received 17 May 2011; revised 28 February 2012; accepted 2 March 2012; published 27 April 2012.

[1] Chemical osmosis is considered a plausible cause of abnormal pressures in shale formations of sedimentary basins. A set of experimental data on chemical osmosis was recently obtained for different shales, mainly in the framework of studies on radioactive waste repositories in deep argillaceous formations. Based on these data, large, osmotically induced overpressures up to tens of MPa were predicted by *Neuzil and Provost* [2009] under appropriate conditions. However, such large overpressures have not been found in sedimentary basins such that the reasons for this disparity between predictions and observations need to be clarified. Accordingly, two natural causes for lower than expected osmotic pressure were investigated: the effect of the complex composition of natural waters, including both monovalent and divalent cations, on the osmotic efficiency and the resulting abnormal pressures, and the presence of steady state rather than transient-state salinity distributions. For this purpose, an electrical triple-layer model accounting for multi-ionic solutions was developed and used to calculate the osmotic efficiency at different proportions of monovalent and divalent cations. The calculated decrease of the osmotic efficiency when  $\text{Ca}^{2+}$  is introduced in a  $\text{Na}^+$ -clay system yields a noticeable decrease in the ability of the shale to generate overpressures. A discussion addresses the generation of abnormal pressures at steady state conditions found in sedimentary basins, i.e., with a linear distribution of the concentration across the formation. The persistence of moderate overpressures was predicted because of the nonlinearity associated with the dependence of the chemo-osmotic efficiency on the concentration and the porosity. Finally, a case study of the moderate excess hydraulic head measured in the Toarcian/Domerian argillaceous formation of Tournemire (SE of France) was investigated. The analysis indicated an osmotic origin for the excess head and illustrated the influence of the pore water composition.

**Citation:** Tremosa, J., J. Gonçalves, and J.-M. Matray (2012), Natural conditions for more limited osmotic abnormal fluid pressures in sedimentary basins, *Water Resour. Res.*, 48, W04530, doi:10.1029/2011WR010914.

### 1. Introduction

[2] Abnormal fluid pressures, which can be defined as a variation in fluid pressure relative to hydrostatic pressure, are frequently encountered in subsurface environments, at a wide range of depths and geological settings [*Chilingar et al.*, 2002]. Interpretation of the origin of abnormal pressures enables information to be obtained on the hydrodynamics in the studied formation [*Neuzil*, 1995]. Osmosis, or fluid flow driven by a chemical potential gradient, is considered a plausible cause of abnormal or nonhydrostatic fluid pressures in sedimentary basins under appropriate conditions [*Marine and Fritz*, 1981; *Neuzil*, 2000; *Gonçalves et al.*, 2004; *Rousseau-Gueutin et al.*, 2009; *Neuzil and Provost*, 2009]. However, debate concerning the osmotic

origin of abnormal pressure continues and the concept is controversial, since few examples are reported and the nature of the process is not well established [*Neuzil and Provost*, 2009].

[3] Overpressures in many basins are not caused by osmosis but rather by a forcing, such as when a portion of the mechanical stress is transferred to fluids [*Neuzil*, 1995, 2003; *Chilingar et al.*, 2002]. Therefore, careful characterization of the geological environment and its related flow and transport processes, coupled with a hydromechanical study are needed to assess the osmotic origin of observed overpressures. However, abnormal fluid pressures due to physical forcing tend to dissipate quickly in a geological sense, and these overpressures are most common in young basins [*Lee and Deming*, 2002; *Gonçalves et al.*, 2004]. An osmotic origin of abnormal pressures can be envisaged in specific geological environments such as in clay-rich and highly compacted formations where a chemical concentration gradient exists and when overpressures persist in old basins [*Marine and Fritz*, 1981; *Neuzil and Provost*, 2009]. A situation presenting a maximum concentration at the center of the formation, with transient-state conditions for

<sup>1</sup>UMR-7619 SISYPHE, UPMC University, Paris, France.

<sup>2</sup>IRSN, DEI/SARG/LR2S, Fontenay-aux-Roses, France.

<sup>3</sup>CNRS, CEREGE, UMR-6635, Aix-Marseille University, Aix en Provence, France.

solute transport and water flow, is most often required for inducing an excess pressure [Neuzil and Provost, 2009].

[4] Osmosis is related to anionic exclusion caused by the negative electrical charges at the clay mineral surface. Osmosis confers membrane behavior to the clay rock, partially impeding solutes but not water molecules crossing the membrane. The osmotic efficiency of a clay rock is expressed through the osmotic efficiency coefficient,  $\varepsilon$ , which ranges between 0 for nonmembrane behavior and 1 for perfect membrane behavior, where solute flux is totally impeded. This coefficient can be determined by experiments, performed in situ in boreholes [Neuzil, 2000; Garavito et al., 2007; Rousseau-Gueutin et al., 2010], or on samples in the laboratory [Cey et al., 2001; Horseman et al., 2007; Rousseau-Gueutin et al., 2009; Tremosa, 2010]. The osmotic efficiency can also be computed in a predictive sense using theoretical models that consider the electrical interactions between the solution and the charged surface together with the petrophysical properties of the porous media [Bresler, 1973; Fritz, 1986; Revil and Leroy, 2004; Gonçalves et al., 2007].

[5] Chemo-osmotic fluid flow is considered in a generalized Darcy's law as follows:

$$q = -\frac{k}{\eta}(\nabla P + \rho_f g \nabla z) + \varepsilon(b, C) \frac{k}{\eta} \nabla \Pi, \quad (1)$$

where  $q$  is the specific discharge ( $\text{m s}^{-1}$ ),  $k$  is the intrinsic permeability ( $\text{m}^2$ ),  $\eta$  is the dynamic viscosity of water ( $\text{Pa s}$ ),  $P$  is the pore pressure ( $\text{Pa}$ ),  $\rho_f$  is the fluid density ( $\text{kg m}^{-3}$ ),  $g$  is the acceleration due to the gravity ( $\text{m s}^{-2}$ ),  $\nabla z$  is (0,0,1) if the  $z$ -axis is directed upward,  $\varepsilon(b, C)$  is the osmotic efficiency dependent on the half-pore size,  $b$  (m), and on the concentration  $C$  ( $\text{mol L}^{-1}$ ), and  $\Pi$  is the osmotic pressure ( $\text{Pa}$ ).

[6] Until recently, few measurements of osmotic efficiency coefficients on natural argillaceous formations were available [Young and Low, 1965], leading to general skepticism regarding the generation of overpressures by osmosis. Some experiments have, however, been carried out over recent years [Neuzil, 2000; Cey et al., 2001; Al-Bazali, 2005; Garavito et al., 2007; Horseman et al., 2007; Rousseau-Gueutin et al., 2009, 2010], leading to a better characterization of chemo-osmotic properties of argillaceous rocks. In particular, these studies clearly show that chemo-osmotic flow exists in such rocks.

[7] In their analysis of these experiments, Neuzil and Provost [2009] predicted overpressures from several bars up to tens of MPa, depending on the petrophysical properties of the clay rock and on the concentration difference across the clay rock. However, such large overpressures attributed to chemical osmosis have not been observed in sedimentary basins. For example, a 1 MPa overpressure that appeared to be caused by chemical osmosis was reported for the Dunbarton Basin [Marine and Fritz, 1981] and an osmosis contribution of 0.1–0.15 MPa to the total overpressure ranging between 0.5 and 0.6 MPa was calculated for the Callovo-Oxfordian of the Paris Basin [Rousseau-Gueutin et al., 2009]. Different explanations for this disparity as reported by Neuzil and Provost [2009] include: shales are less osmotically efficient than suggested and the commonly used Bresler [1973] predictive model is perhaps conceptually

flawed, even though it was fitted mostly on experimental data. However, Neuzil and Provost [2009] have argued that this is probably not the real cause of disparity since large pressures were generated by osmosis in laboratory tests. Also, argillaceous formations are ineffective membranes at a large scale and osmotic efficiencies measured at a small scale on samples and in boreholes cannot be upscaled to the formation scale. In particular, this statement is supported by the fact that osmotic efficiency is expected to disappear when a connected fracture network is present in the clay rock [Swarbrick and Osborne, 1998; Chilingar et al., 2002]. However, similar hydraulic permeabilities are found at both the small and large scale, indicating an absence of short-circuiting [Neuzil, 1994]. In addition, the conditions for the generation of overpressures by osmosis are rare; and last, osmotic overpressures are not systematically studied when an abnormal pressure is encountered in a basin.

[8] Other natural causes for lower than expected osmotic overpressures, not previously considered, are examined in this paper. The first cause pertaining to the effect of a more complex pore water composition than the simple NaCl solution typically considered, i.e., including both monovalent and divalent solutes, is analyzed. The second cause pertains to basin salinity distribution existing at quasi-equilibrium (steady state fluxes) as opposed to transient-state, which is commonly assumed. The resulting pressure fields are identified. Finally, the origin of the moderate excess hydraulic head measured in a Toarcian/Domerian argillaceous formation, studied at the Tournemire IRSN underground research laboratory (SE of France), is investigated. Chemical osmosis is addressed as a cause and the influence of pore water composition on the osmotic process in the formation is analyzed.

## 2. Effect of Mixed Ca/Na Solutions on the Osmotic Efficiency and Abnormal Pressures

[9] Theoretical and experimental studies of chemical osmosis in pure clays and argillaceous rocks have typically been conducted using pure NaCl or CaCl<sub>2</sub> solutions (see compilations by Bresler [1973] and Neuzil and Provost [2009]), rather than more complex solutions containing both monovalent and divalent solutes. The osmotic efficiency coefficient is significantly lower with Ca<sup>2+</sup> than with Na<sup>+</sup> solutions [Bresler, 1973]. In particular, Shackelford and Lee [2003] measured destruction of the membrane potential of a Na-bentonite induced by the replacement of the Na<sup>+</sup> interlayer cations by Ca<sup>2+</sup>. However, the osmotic efficiency coefficient of clay rocks with a mix of Na<sup>+</sup> and Ca<sup>2+</sup> solutions is unknown. Because natural waters have complex compositions, the osmotic efficiency is expected to be affected according to their composition. Such effects on abnormal fluid pressure are evaluated in the following discourse.

### 2.1. Model for Osmotic Efficiency Calculations With Mixed Ca/Na Solutions

[10] Chemical osmosis occurs in clay rocks because of anion exclusion, which results from ionic transport restrictions due to size and/or electrical effects (and salinity, consequently). Anion exclusion and, thus, osmotic efficiency are particularly efficient when clay is highly compacted and the electrical diffuse layers overlap [Bolt, 1979]. Calculations of the osmotic efficiency will consequently

depend on the mean content of anions in the clay pores,  $\langle \overline{C^-} \rangle$ , and on the anion content in the bulk water,  $C_f$ . A simplified relationship expressing these factors is [Kemper and Rollins, 1966; Bresler, 1973; Bolt, 1979]:

$$\varepsilon = 1 - \frac{\langle \overline{C^-} \rangle}{C_f}. \quad (2)$$

A more complex expression is obtained by the resolution of the Navier-Stokes equation integrating the chemical force (Appendix A equation (A16)). This expression requires knowledge of the ion distribution in the pores related to the clay surface and its dependence on the pore size, which can be calculated using an electrical triple-layer model (TLM). In Appendix A, a TLM that accounts for multi-ionic solutions and interacting adjacent diffuse layers (compacted clay rocks with low pore size) is developed.

[11] The TLM is calibrated against osmotic experimental data from experiments on natural clay rocks [Neuzil, 2000; Cey et al., 2001; Al-Bazali, 2005; Garavito et al., 2006, 2007; Horseman et al., 2007; Rousseau-Gueutin et al., 2009, 2010]. Comparison of predicted osmotic efficiencies

using the TLM with measured osmotic efficiencies for NaCl-clay systems is shown in Figure 1, as a function of the product of the half-pore size,  $b$  (in nm), and the chloride concentration in the bulk solution,  $C_f$  (in mol L<sup>-1</sup>), or  $b \times C_f$ . This representation illustrates the combined effect of the pore size and the salinity, which modify the electrical potentials and lead to transport restrictions (e.g., Bresler [1973]; Gonçalves et al. [2007]). The half-pore size,  $b$  (m), for clay rocks can be determined by a mass balance equation based on a plane-parallel geometry assumption, as follows [Neuzil, 2000; Neuzil and Provost, 2009; Gonçalves et al., 2010]:

$$b = \frac{\omega}{\rho_s A_s (1 - \omega)}, \quad (3)$$

where  $\omega$  is the porosity,  $\rho_s$  is the grain density (g m<sup>-3</sup>), and  $A_s$  is the specific surface area (m<sup>2</sup> g<sup>-1</sup>).

[12] A fairly good agreement is observed in Figure 1 between the TLM results and the data for natural clay rocks. There is significant scatter in measured values of  $\varepsilon$  lower than 0.08. Thus, the TLM can provide a relatively good estimation of osmotic efficiency in clay rock systems

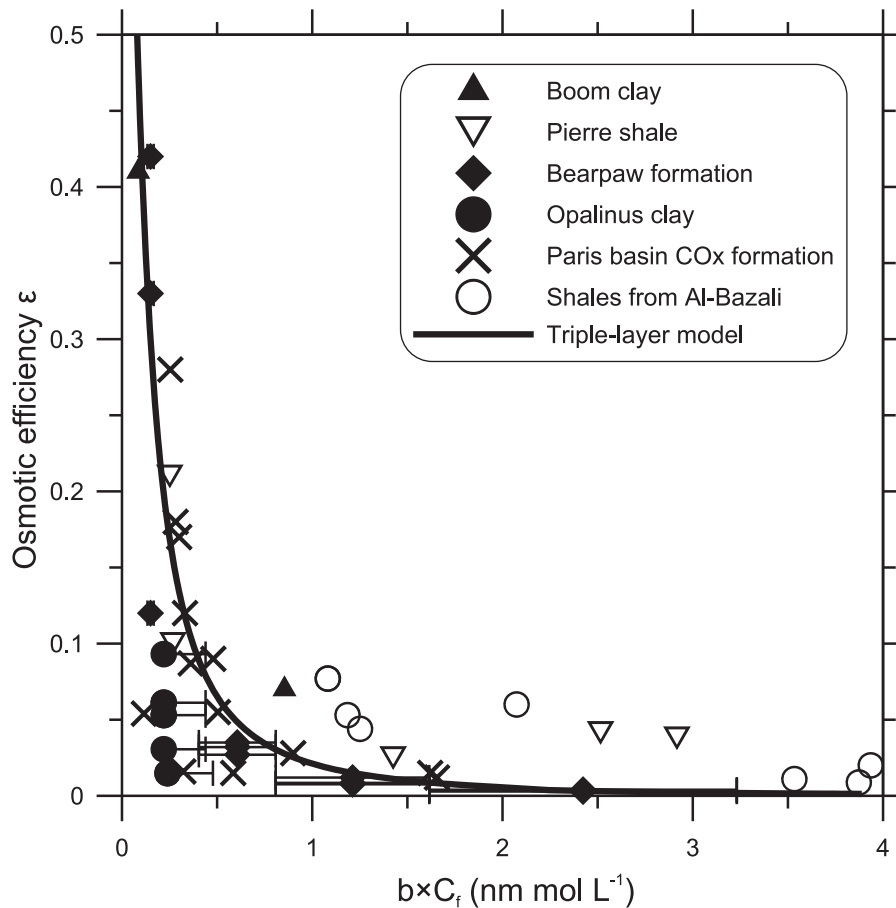


**Figure 1.** Model and data from several argillaceous formations of chemo-osmotic efficiency coefficient as a function of  $b \times C_f$  for a NaCl-clay system. Data from Oligocene Boom clay [Garavito et al., 2007], Cretaceous Pierre shale [Neuzil, 2000; Al-Bazali, 2005; Garavito et al., 2006], Cretaceous Bearpaw formation [Cey et al., 2001; Hendry and Wassenaar, 1999], Jurassic Opalinus clay [Boisson, 2005; Horseman et al., 2007], Paris basin Callovo-Oxfordian (COx) formation [Rousseau-Gueutin et al., 2009, 2010], and shales from Al-Bazali [Al-Bazali, 2005; Neuzil and Provost, 2009].

with  $b \times C_f$  values below  $1 \text{ nm mol L}^{-1}$ , but the estimation is less accurate for systems with higher  $b \times C_f$ . The main uncertainty on the use of the TLM stems from the absence of osmotic experiments performed on natural clay rocks with pure  $\text{Ca}^{2+}$  solution or  $\text{Na}^+/\text{Ca}^{2+}$  mixed solutions to validate the osmotic efficiencies calculated for solutions different to  $\text{Na}^+$  solutions.

[13] Most natural water concentrations and compositions can be considered in the TLM accounting for diffuse layers truncation and multi-ionic solutions. For high salinities, diffuse layers in the pores collapse and membrane behavior of the clay rock almost vanishes [Mitchell and Soga, 2005]. Positive surface electrical potentials are, therefore, calculated by the TLM in this situation at the limit of validity of the model since it can only consider negatively charged surfaces. For instance, for a simple NaCl solution and  $b$  of 4 nm, this limit corresponds to a  $C_f$  of  $0.5 \text{ mol L}^{-1}$ .

## 2.2. Effect of Mixed Ca/Na Solutions on Osmotic Efficiency

[14] In order to determine the chemical osmotic efficiency for mixed  $\text{Na}^+/\text{Ca}^{2+}$  solutions, calculations are performed for varying solution compositions with the TLM presented in Appendix A. Changes in solution composition are introduced according to a ratio  $2 \times \text{Ca}^{2+}/(\text{Na}^+ + 2 \times \text{Ca}^{2+})$ , expressed in molal units, which varies from 0 for a pure Na solution to 1 for a pure Ca solution. This ratio is denoted hereafter as the calcium index (CaI). Figure 2 shows the osmotic efficiency ( $\epsilon$ ) as a function of the CaI and  $b \times C_f$ . Figure 2 illustrates that  $\epsilon$  decreases as the salinity ( $C_f$ ) and/or the pore size ( $b$ ) increase, and when the

counterions are  $\text{Ca}^{2+}$  versus  $\text{Na}^+$ . At large pore size and for high bulk concentration, the electrical double layer collapses resulting in weak anionic exclusion. For example, the osmotic efficiency calculated for a CaI of 0.1 (which corresponds to a Na/Ca ratio of 18:1, in molar units) is approximately half the efficiency for a CaI of 0. Furthermore, large osmotic efficiency values, i.e.,  $\epsilon$  close to 1, cannot be reached for CaI higher than 0.25, corresponding to a Na/Ca ratio of 6:1. For pure  $\text{CaCl}_2$  solutions, the maximum calculated  $\epsilon$  values are slightly below 0.5, when very low pore sizes and low-salinity waters are considered. These observations suggest that introducing  $\text{Ca}^{2+}$ , even in low amounts, into a Na-clay system will induce a dramatic decrease in osmotic efficiency and a reduction in the membrane behavior of the clay. Consequently, an osmotic efficiency determined experimentally using NaCl solutions will probably overestimate the osmotic efficiency under natural conditions.

## 2.3. Implications of Mixed Ca/Na Solutions for Overpressures

[15] Generation of abnormal pressures in a sedimentary basin by osmosis can only occur in low permeability or hydraulically isolated layers [Chilingar *et al.*, 2002]. Furthermore, in the presence of permeable connections, such as fracture networks, abnormal pressure generation will be impossible due to the dominance of fracture flow relative to osmotic flow. The situation encountered in sedimentary basins as illustrated in Figure 3 is particularly favorable to generating overpressures by osmosis. It consists of an argillaceous layer surrounded by two aquifer layers, with the

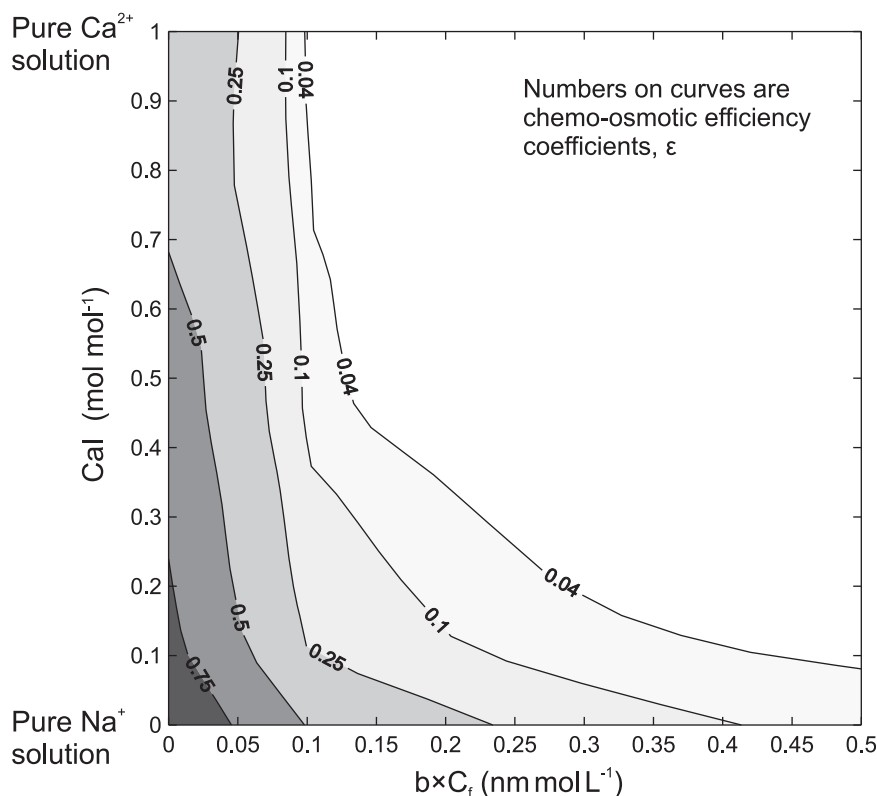


**Figure 2.** Evolution of chemo-osmotic efficiency coefficient calculated with the TLM as a function of the calcium index (CaI),  $2 \times \text{Ca}^{2+}/(\text{Na}^+ + 2 \times \text{Ca}^{2+})$ , and  $b \times C_f$ .

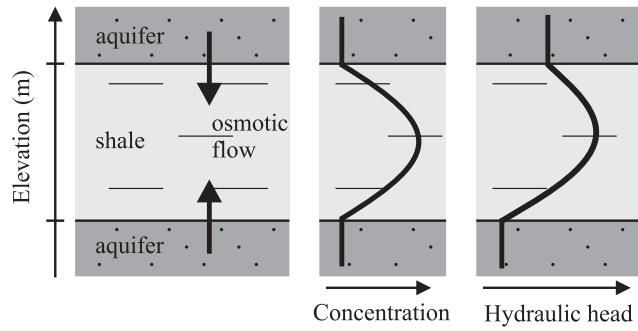


**Figure 3.** Diagram of abnormal pressure generation by osmosis due to a salinity gradient between the shale layer and the surrounding aquifers.

porosity initially filled by connate seawater entrapped during sedimentation. During basin evolution and especially during aquifer outcropping, saline pore water in the aquifers is flushed by freshwater, but not the clay rock pore water due to conductive flow inefficiency. A salinity gradient between the argillaceous formation and the aquifers is thus established and tends to equilibrate over time through diffusion [e.g., *Pearson et al.*, 2003; *Patriarche et al.*, 2004; *Neuzil and Provost*, 2009; *Mazurek et al.*, 2011]. If the argillaceous formation exhibits membrane properties, the salinity gradient causes osmotic flow directed toward the formation with higher salinity (i.e., toward the center of the clay rock upward from the lower aquifer and downward from the upper aquifer). This osmotic flow generates a pressure buildup in the clay rock to a quasi-equilibrium, corresponding to  $q \simeq 0$  in equation (1).

[16] Let us now consider a horizontal argillaceous formation surrounded by two aquifer layers, with only vertical fluid flow in the shale layer and a salinity gradient in the argillaceous formation. According to the scenario in Figure 3,  $C_{\max}$  and  $C_{\min}$  are the concentrations ( $\text{mol L}^{-1}$ ) at the center of the shale layer and at aquifer-shale boundaries, respectively. The resulting abnormal pressure is calculated in a similar way as *Neuzil and Provost* [2009], accounting for osmotic efficiency dependence to concentration. Assuming a constant pore size ( $b = 4$  nm), an expression of the abnormal pressure,  $P_0$  (Pa), is obtained, dependent on the concentration difference through  $\varepsilon(C)$ , but not on the formation thickness [*Neuzil and Provost*, 2009], as follows:

$$P_0 = \int_{C_{\max}}^{C_{\min}} \varepsilon(C) \frac{d\Pi}{dC} dC. \quad (4)$$

$P_0$  corresponds to the nonhydrostatic pressure, such that  $P_0 = 0$  for hydrostatic pressures,  $P_0 > 0$  for overpressures, and  $P_0 < 0$  for abnormal low pressures. Osmotic pressure is expressed according to the Van't Hoff relation, or  $\Pi = \nu RTC$ , which holds for solutions with concentrations lower than  $1 \text{ mol L}^{-1}$  [*Fritz*, 1986], where  $\nu$  is the number of ionic species (e.g.,  $\nu = 2$  for NaCl and  $\nu = 3$  for  $\text{CaCl}_2$ ),  $R$  is the universal gas constant ( $8.314 \text{ m}^3 \text{ Pa K}^{-1} \text{ mol}^{-1}$ ), and  $T$  is the absolute temperature (K).

[17] In order to evaluate the influence of natural solutions with both monovalent and divalent cations on osmotically generated pressures,  $P_0$  is calculated for solutions

with various proportions of  $\text{Ca}^{2+}$  and  $\text{Na}^+$ , as a function of the concentration gradient and the half-pore size. The TLM accounting for multi-ionic solutions (Appendix A) is used to calculate the osmotic efficiency as a function of salinity, solution composition, and pore size. Results for a concentration ratio  $C_{\max}/C_{\min}$  of 10 and CaI values ( $\text{CaI} = 2 \times \text{Ca}^{2+}/(\text{Na}^+ + 2 \times \text{Ca}^{2+})$ ) of 0, 0.1, 0.2, 0.5, and 1 are depicted in Figure 4. Note that both concentration ratio ( $C_{\max}/C_{\min}$ ) and difference ( $C_{\max} - C_{\min}$ ) have to be specified to establish Figure 4. Indeed,  $P_0$  depends not only on the concentration difference but also on the  $C_{\max}$  and  $C_{\min}$  values because of  $\varepsilon$  dependence on the concentration. The half-pore size range of 1 to 10 nm used in Figure 4 corresponds to a porosity ranging between 0.1 and 0.5, using equation (3) and average values of the specific surface area and grain density for compacted clay rocks of  $40 \text{ m}^2 \text{ g}^{-1}$  and  $2700 \text{ kg m}^{-3}$ , respectively [*Boisson*, 2005].

[18] In the case of a pure NaCl solution (Figure 4a), moderate overpressures are generated by osmosis, ranging between some tens of kPa to 1 MPa, as a function of the half-pore size and the salinity difference,  $C_{\max} - C_{\min}$ . The highest overpressure is obtained for a half-pore size close to 1 nm and, conversely,  $P_0$  values lower than  $\sim 0.1$  MPa are obtained for a half-pore size greater than 5 nm.

[19] The dependence on the concentration of the osmotic efficiency is illustrated by the trend in  $P_0$  values with increasing concentration differences for given  $b$ . With a salinity increase, the osmotic flow and its related overpressure tends to increase due to the increase in concentration difference but, inversely,  $\varepsilon$  decreases with the salinity increase and tends to lower the osmotic flow. Thus, for the same half-pore size, the calculated overpressure,  $P_0$ , first increases with increasing concentration difference but eventually decreases when higher concentration differences are considered.

[20] Comparison of the calculated overpressures for various values of CaI (e.g., Figure 4a versus Figure 4e) indicates a strong decrease in  $P_0$  with increasing  $\text{Ca}^{2+}$  concentration compared to  $\text{Na}^+$ . This decrease is observed even for solutions with a low CaI of 0.1 (Figure 4b), and  $P_0$  further decreases as the  $\text{Ca}^{2+}$  proportion increases. The highest  $P_0$  of 1 MPa occurs for a CaI of 0 (Figure 4a), and  $P_0$  decreases to 0.8 MPa for a CaI of 0.1 (Figure 4b), to 0.4 MPa for a CaI of 0.2 (Figure 4c), to 0.1 MPa for a CaI of 0.5 (Figure 4d), and to only 0.015 MPa for a CaI of 1 (Figure 4e). These results suggest that chemical osmosis is unable to generate significant overpressures for pure  $\text{Ca}^{2+}$  solutions. For mixed  $\text{Ca}^{2+}/\text{Na}^+$  solutions, overpressures are expected to be more moderate than for pure  $\text{Na}^+$  solutions.

## 2.4. Discussion

[21] The interactions between the charged surface of the clay and the pore water were represented using a TLM accounting for diffuse layers overlapping and multi-ionic solutions. The results of the model simulations revealed a decrease in osmotic efficiency with increasing  $\text{Ca}^{2+}$  in solution compared to  $\text{Na}^+$  solutions, even with low proportions of  $\text{Ca}^{2+}$ . Since the values of CaI in pore waters of natural shales are  $\sim 0.1$  and  $0.2$  [*Pearson et al.*, 2003; *Vinsot et al.*, 2008], the ability of natural buildup of large overpressures by osmosis appears consequently reduced by the osmotic efficiency degradation with the pore water composition.

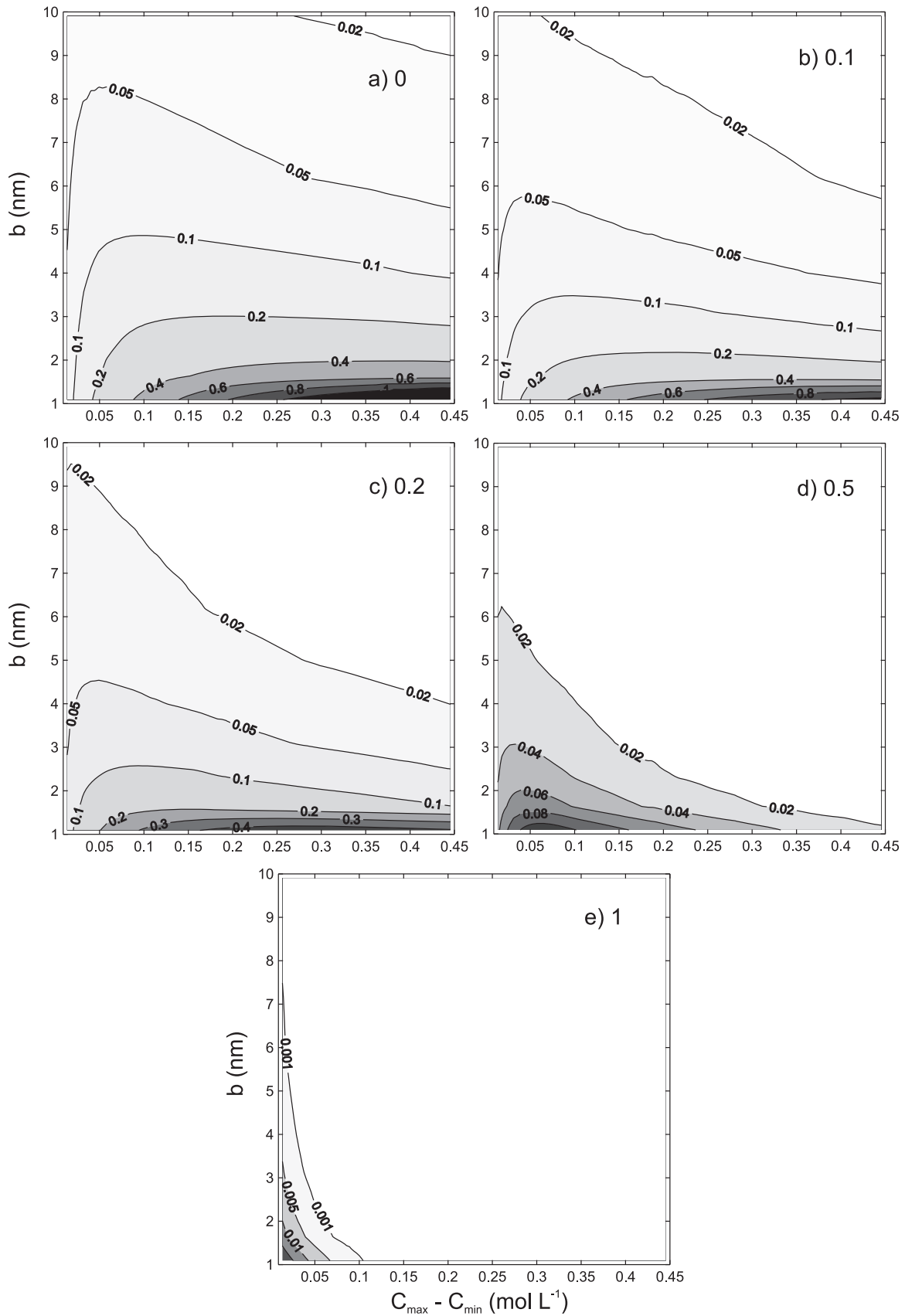


**Figure 4.** Overpressures ( $P_0$  in MPa) generated by chemical osmosis as a function of the concentration difference,  $C_{\max} - C_{\min}$ , with  $C_{\max}/C_{\min} = 10$  and the pore size,  $b$ , for different values of the calcium index (CaI) (a) 0, (b) 0.1, (c) 0.2, (d) 0.5, and (e) 1. Numbers on curves are  $P_0$ .

This reduction in the osmotic efficiency may explain the scarcity of observed overpressures linked to osmosis. However, uncertainties in the predictive model preclude concluding that this effect is the only cause of apparent discrepancies. The fact remains that the effect of mixed monovalent/divalent solutions appears important for the interpretation of abnormal pressures generated by osmosis in clay rocks.

### 3. Abnormal Fluid Pressures Generation at Steady State

[22] Abnormal fluid pressures generated by osmosis have thus far been associated exclusively with transient salinity distributions, where the abnormal pressures will evolve with the salinity profile across the argillaceous formation, e.g., by solute diffusion toward the surrounding aquifers (Figure 3). However, because of the dependence of osmotic efficiency on the concentration and half-pore size, i.e., the nonlinearity of the osmotic efficiency, any variations in the argillaceous formation of the concentration or the porosity will change the osmotic efficiency value. These changes in  $\varepsilon$  can lead to abnormal pressures, even when the salinity gradient is at steady state and the basin is at equilibrium. The abnormal pressure profile merely fulfills constant fluid flow by balancing the osmotic and hydraulic components of the fluid flow.

[23] For example, abnormal fluid pressure can be calculated by solving the continuity equation at steady state, considering that fluid flow is entirely vertical across a shale, or

$$\frac{\partial}{\partial z} \left[ \rho_f \frac{k}{\eta} \left( \frac{\partial P}{\partial z} + \rho_f g \right) - \rho_f \varepsilon(b, C) \frac{k}{\eta} \frac{\partial \Pi}{\partial z} \right] = 0. \quad (5)$$

The resolution of this equation requires determining relevant hydraulic parameters. Intrinsic permeability can be obtained using Poiseuille's law for a plane, parallel pore geometry as follows [Walsh and Brace, 1984]:

$$k = \frac{b^2}{3 \omega^{-m}}, \quad (6)$$

where  $b$  is in meters and  $m$  is the cementation factor, estimated at 2.3 for natural shales [Tremosa, 2010]. Fluid density  $\rho_f$  and dynamic viscosity  $\eta$  are considered constant across the formation at values of  $1000 \text{ kg m}^{-3}$  and  $10^{-3} \text{ Pa s}$ , respectively.

[24] Two scenarios for abnormal pressure calculations at steady state were tested using plausible salinity and pore size variations across a 100-m thick argillaceous formation, considering a linear hydrostatic pressure gradient. The first case (Figure 5) considers a formation with a linear concentration profile (between  $10^{-1}$  and  $10^{-3} \text{ mol L}^{-1}$  of pure NaCl solution) with higher concentrations in the deeper part, as salinity generally increases with depth in sedimentary basins [de Marsily, 1986], and a constant porosity of 0.2. Salinity profiles are generally transient in argillaceous sequences in sedimentary basins [Mazurek et al., 2011], but linear salinity profile with steady state diffusion process are also sometimes observed, such as in the Boom Clay at Essen in Belgium [Mazurek et al., 2011]. Taking into

account a linear salinity profile makes it possible to identify the individual effect of salinity variations on osmotic flow and associated pressures. Half-pore size is calculated using equation (3), assuming a constant specific surface area of  $40 \text{ m}^2 \text{ g}^{-1}$  and a grain density of  $2700 \text{ kg m}^{-3}$ , average values for compacted clay rocks [Boisson, 2005], yielding a value for  $b$  of 2.3 nm. The osmotic efficiency can then be calculated as a function of the concentration and the half-pore size using the TLM (Appendix A) for pure NaCl solutions.

[25] According to the concentration variation across the formation, osmotic efficiency is higher at the upper part of the formation, inducing differences in osmotic flow in the formation leading to a limited pressure buildup of 0.04 MPa (Figure 5). The resulting overall flow in the argillaceous formation, calculated using equation (1), is directed downward and is dominated by osmotic flow in comparison to purely hydraulic flow.

[26] In the second case (Figure 6), in addition to the previous linear concentration profile, a linear porosity variation (between 0.15 and 0.2), with a lower value in the deeper part due to higher compaction, was considered. This porosity variation corresponds to the maximal vertical porosity variations for a 100-m thick shale layer predicted by porosity-depth functions [Magara, 1980]. Porosity range corresponds to a half-pore size extending from 1.6 to 2.3 nm. The resulting osmotic efficiency variations across the formation are more complex because  $\varepsilon$  increases with decreasing concentration, but it also decreases when the pore size increases. These changes lead to a higher-pressure buildup than in the previous case with concentration variations only. Therefore, an overpressure of  $\sim 0.075$  MPa is obtained at steady state. This overpressure is slightly lower than the overpressure predicted at transient state (Figure 4) for similar pore size and concentration gradient. The overall flow is, as in the previous case, directed downward. The influence of intrinsic permeability variations related to porosity changes across the formation was also evaluated by calculating the pressure buildup considering constant permeability instead of variable permeability. In such conditions, a more limited overpressure of  $\sim 0.025$  MPa is obtained (Figure 6), illustrating the influence of both osmotic efficiency and intrinsic permeability in the osmotic flow term in equation (1).

[27] Although limited, osmosis can generate overpressures at steady state, i.e., in basins at equilibrium, contrary to the commonly accepted idea that osmotic overpressures can only develop at a transient state on account of the nonlinearity of osmotic efficiency. With only variations in concentration, a weak overpressure is calculated. This overpressure is almost undetectable in an argillaceous layer, because of pressure measurement difficulties in such rocks. With both concentration and pore size variations, a more noticeable overpressure is obtained though slightly lower than the overpressures obtained at transient state. Fairly important differences in the calculated overpressures are observed when limited variations of concentration and flow coefficients ( $k$  and  $\varepsilon$ ) are considered across the shale layer. Identifying these variations in concentration and porosity and considering the nonlinearity of the osmotic efficiency (and other flow coefficients), are thus crucial for understanding overpressures.

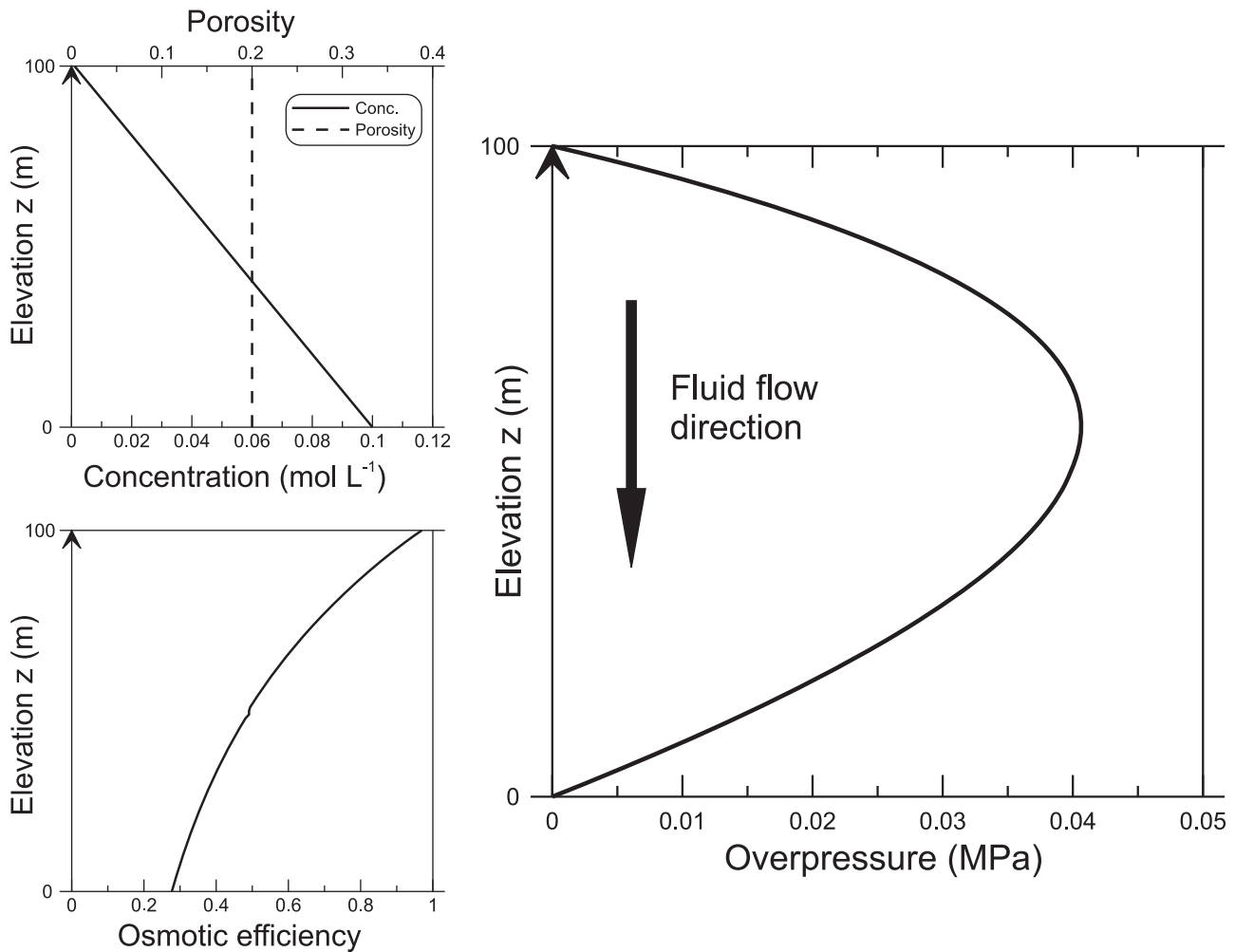


**Figure 5.** Pressure profile across a 100-m-thick argillaceous formation calculated at steady state by chemical osmosis caused by variations in osmotic efficiency with concentration at constant porosity.

#### 4. Influence of Chemical Osmosis on the Excess Hydraulic Head Measured in Toarcian/Domerian Argillaceous Formation of Tournemire (France)

[28] An illustration of the effect of pore water composition on an osmotically partly induced pressure profile can be made by considering the pressure field measured in the Toarcian/Domerian argillaceous formation of Tournemire (SE of France), studied at the IRSN underground research laboratory (URL). For this purpose, we extended the notion of excess pressure expressed in terms of excess head. Indeed, an excess head in the argillaceous sequence is considered herein as a hydraulic head which derives from the linear head profile given by the heads measured in two aquifers surrounding the sequence when purely hydraulic flow at steady state with constant permeability is considered.

[29] The Toarcian/Domerian argillaceous formation of Tournemire is part of the Mesozoic Grands Causses Basin and has a thickness of 250 m of shales and marls at the URL location. The shale is surrounded by two karstic limestone aquifers of Carixian and Aaleanian ages. Since sedimentation ceased in the basin at the end of the Jurassic, the basin evolved under subaerial conditions leading to the

erosion of 800–1600 m of material during the Cretaceous [Peyaud *et al.*, 2005] and karst development in limestone layers [Ambert and Ambert, 1995; Simon-Coignon and Schmitt, 1999]. Major uplifts occurred during the Pyrenean orogenesis in the Eocene and canyon incision mainly occurred during the Miocene.

[30] The identification of the hydraulic head profile across the formation (Figure 7) was determined from pressure measurements in equipped boreholes [Tremosa, 2010]. These measurements were selected outside of the depressed zone induced by the URL [Matray *et al.*, 2007] and are considered to be representative of the formation fluid pressure because they are constant over a sufficiently long time period. A moderate excess hydraulic head of  $\sim 30$  m is apparent (between 20 and 40 m, depending on the boreholes; Figure 7), compared to the linear profile bounded by aquifer heads characterizing purely hydraulic flow at steady state conditions using a constant permeability. This excess head is moderate so that the head in the shale layer does not exceed the head in the overlying aquifer and, thus, cannot be strictly considered as an overpressure. However, because of its nonlinear shape, crucial hydrodynamic information can be obtained studying the nonlinear profile.

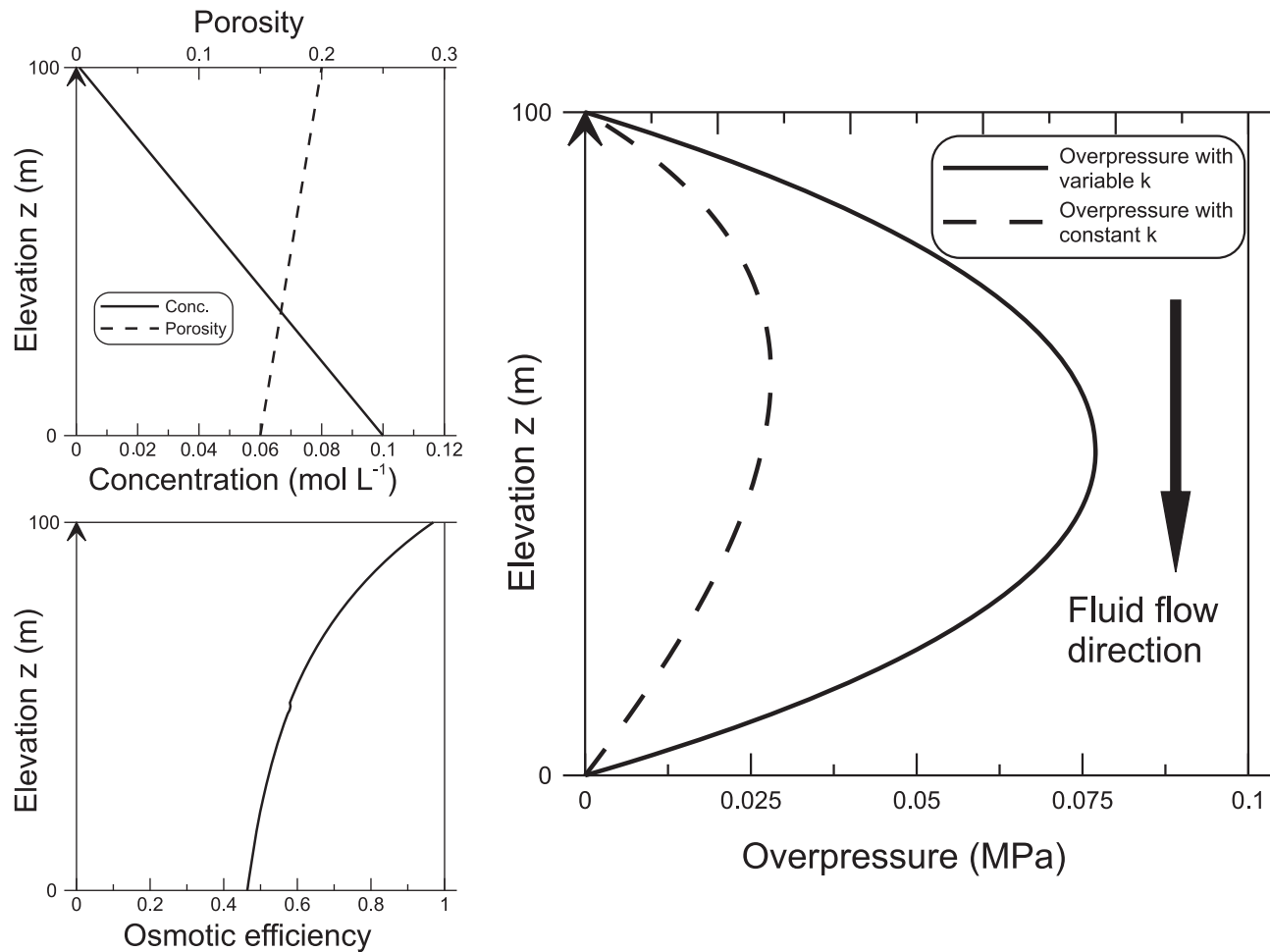


**Figure 6.** Pressure profile across a 100-m-thick argillaceous formation calculated at steady state by osmosis caused by osmotic efficiency variations with both concentration and porosity.

[31] Causes of excess head linked to basin history, such as compaction disequilibrium, tectonic compression, viscoplastic behavior of clays or changes in hydraulic boundary conditions to explain the excess head that exists in the Tournemire argillaceous formation can be discarded. Indeed, because of the basin evolution and valley incision age and because of the present exhumation of the massif, these processes are not relevant for the actual pressure profile interpretation [Tremosa, 2010]. Conversely, chemical osmosis was suspected to be a plausible cause of excess head because the clay-rich content and low porosity of the Toarcian/Domerian shale confers membrane behavior to the formation and on account of the observed concentration profile in the formation with a higher salinity in its center (Figure 8).

[32] In the Toarcian/Domerian argillaceous formation of Tournemire, the intrinsic permeability measurements considered as representative of the undisturbed rock [Boisson *et al.*, 2001; Bertrand *et al.*, 2002] range between  $10^{-21}$  and  $10^{-20}$  m<sup>2</sup>. In such an impervious rock, measuring permeability with an accuracy below one order of magnitude is difficult [Neuzil, 1994]. However, permeability variations are suggested by the measurable porosity profile. The mean value of porosity is 9% and ranges from 2.7% in the lower

Toarcian to 11.1% in the upper part of the upper Toarcian. Porosity and measured and calculated permeability variations across the formation are depicted in Figure 8. Intrinsic permeability was calculated using equation (6), where the half-pore size was estimated using equation (3). The porosity was determined by measurements of water content and volume [Matray *et al.*, 2007], the grain density by helium pycnometry, and the specific surface area by the Brunauer, Emmett, and Teller (BET) method. Parameter profiles are listed in Table 1.

[33] The membrane behavior of the Toarcian/Domerian clay rock of Tournemire has been demonstrated by a set of laboratory experiments on samples using NaCl solutions [Tremosa, 2010]. Measured chemo-osmotic efficiencies ranged from 0.014 to 0.31 for salinity gradients between 5 and 18, using the formation salinity as the reference salinity in these experiments. However, measurements at only one elevation impede the osmotic efficiency profile being established from these measurements. The osmotic efficiency profile was then calculated using the TLM presented in Appendix A, and using pore size and pore water composition as input parameters. The pore water composition was calculated by a thermodynamic geochemical model which aims to reproduce the rock-pore water interactions

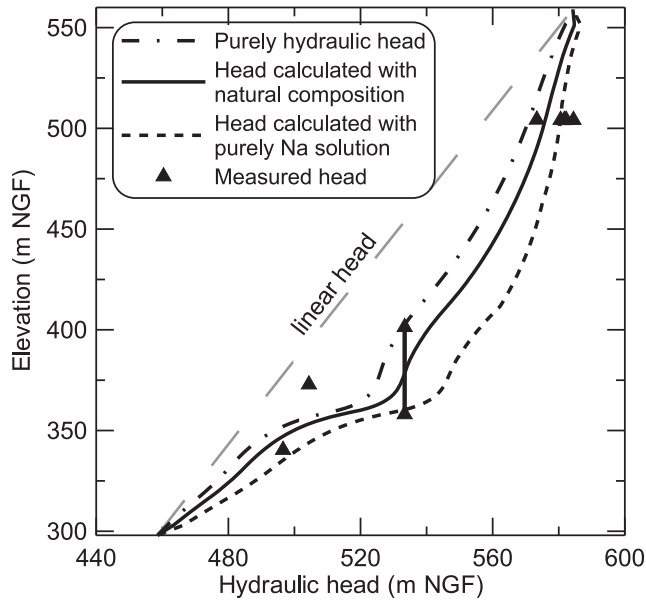


**Figure 7.** Measured and calculated hydraulic head profiles in the Toarcian/Domerian argillaceous formation of Tournemire.

[Tremosa *et al.*, 2012]. This geochemical model requires the measured  $\text{Cl}^-$  and  $\text{SO}_4^{2-}$  mobile anion profiles, which give the pore water salinity, and calculates the cation contents as a function of the interactions with the rock (mineral saturation and cation exchange). For the sake of simplicity, monovalent cations were assumed to be  $\text{Na}^+$ , divalent cations assumed to be  $\text{Ca}^{2+}$ , and anions assumed to be  $\text{Cl}^-$  (Figure 8). The TLM developed in this study can account for multi-ionic solutions and, thus, the osmotic efficiency was calculated as a function of the solution composition (Table 1).

[34] The hydraulic head profile in the Toarcian/Domerian argillaceous formation was calculated in 1-D, along the  $z$ -axis, at steady state (equation (5)) considering purely Darcian flow and chemical osmosis. Hence, the excess head buildup was calculated for a given concentration

profile, considering the system in pseudo-equilibrium at each time ( $q \simeq 0$ ). The steady state hypothesis avoided reconstructing the flow and transport history in the basin. This assumption was supported by the very low filtration and mass transport flux rates in the formation. The measured heads in the surrounding Carixian and Aalenian aquifers were introduced as boundary conditions and the present-day composition profile as chemical forcing (Figure 8). Purely hydraulic flow with constant permeability leading to a linear hydraulic head profile represents the reference state. Then, two calculations were performed: purely hydraulic flow with variable hydraulic permeability, and hydraulic and osmotic flows with chemo-osmotic efficiency and vertical permeability variations. The calculated head obtained taking into account purely hydraulic flow with permeability variations is shown in Figure 7 and presents an important deviation compared with the reference linear head profile obtained using a constant permeability. Indeed, the calculated hydraulic head profile, where permeability variations were considered, can almost reproduce the measured excess head. The deviation from the measured excess head,  $\sigma$ , can be quantified as follows:

$$\sigma = \frac{|\Delta h_{\text{data}} - \Delta h_{\text{model}}|}{\Delta h_{\text{data}}} \times 100, \quad (7)$$

where  $\Delta h_{\text{data}}$  and  $\Delta h_{\text{model}}$  are, respectively, the measured and the calculated excess heads relative to the linear head profile. The value of  $\sigma$  was 24% for the head obtained taking into account purely hydraulic flow and variable permeability.

[35] The calculations of the hydraulic head profiles accounting for hydraulic flow and chemical osmosis together were performed using the osmotic efficiency profile calculated from pore water composition, as well as using an osmotic efficiency profile calculated for a NaCl solution at the same salinity (Table 1). Use of these two osmotic efficiency profiles enables the influence of pore water composition on the osmotic excess head to be evaluated. The two calculated hydraulic head profiles are depicted in Figure 7, together with the measured hydraulic heads.

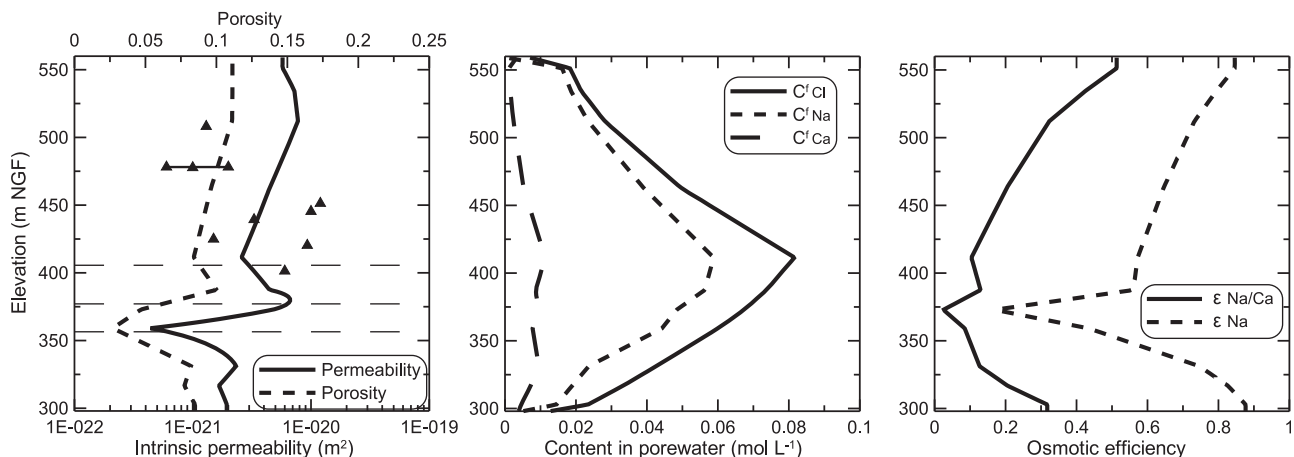


**Figure 8.** Profiles of intrinsic permeability, porosity, pore water composition, and osmotic efficiency in the Toarcian/Domerian argillaceous formation of Tournemire. Triangles are the measured intrinsic permeabilities [Boisson *et al.*, 2001; Bertrand *et al.*, 2002].

**Table 1.** Parameters Used in the Calculations for the Argillaceous Formation of Tournemire<sup>a</sup>

Formation Unit	Elevation	$\omega_{\text{tot}}$	$\rho_s$	$A_s$	$b$	$\varepsilon_{\text{natural}}$	$\varepsilon_{\text{NaCl}}$
Upper Toarcian	551.3	0.111 ± 0.0006	2.732 ± 0.0005	28 ± 2	1.64 ± 0.12	0.513 [0.493–0.537]	0.846 [0.831–0.863]
Upper Toarcian	534.4	0.111 ± 0.0006	2.721 ± 0.0005	25 ± 2	1.84 ± 0.15	0.425 [0.400–0.452]	0.794 [0.771–0.817]
Upper Toarcian	512.2	0.111 ± 0.0005	2.723 ± 0.0004	24 ± 2	1.91 ± 0.16	0.323 [0.299–0.351]	0.733 [0.704–0.762]
Upper Toarcian	463.1	0.096 ± 0.0006	2.709 ± 0.0005	23 ± 2	1.71 ± 0.14	0.204 [0.183–0.229]	0.646 [0.608–0.687]
Upper Toarcian	411.5	0.084 ± 0.0006	2.735 ± 0.0004	22 ± 2	1.52 ± 0.13	0.104 [0.089–0.122]	0.572 [0.522–0.626]
Int. Toarcian	387.5	0.100 ± 0.0006	2.734 ± 0.0007	25 ± 2	1.63 ± 0.17	0.129 [0.109–0.158]	0.560 [0.503–0.626]
Lower Toarcian	372.9	0.047 ± 0.0006	2.424 ± 0.0028	5 ± 0	4.06 ± 0.07	0.025 [0.024–0.025]	0.169 [0.165–0.175]
Lower Toarcian	359.1	0.027 ± 0.0007	2.385 ± 0.0010	5 ± 0	2.32 ± 0.06	0.085 [0.081–0.089]	0.435 [0.423–0.448]
Domerian	331.2	0.082 ± 0.0006	2.740 ± 0.0007	22 ± 2	1.48 ± 0.05	0.127 [0.120–0.134]	0.746 [0.729–0.761]
Domerian	316.7	0.077 ± 0.0006	2.733 ± 0.0006	23 ± 2	1.34 ± 0.13	0.206 [0.185–0.236]	0.827 [0.796–0.865]
Domerian	302.9	0.085 ± 0.0006	2.737 ± 0.0005	26 ± 2	1.30 ± 0.13	0.317 [0.290–0.348]	0.876 [0.851–0.903]

<sup>a</sup> $\omega_{\text{tot}}$  is the total porosity,  $\rho_s$  is the grain density ( $\text{g cm}^{-3}$ ),  $A_s$  is the specific surface area ( $\text{m}^2 \text{g}^{-1}$ ),  $b$  is the half-pore size (nm),  $\varepsilon_{\text{natural}}$  is the osmotic efficiency calculated for the natural pore water composition, and  $\varepsilon_{\text{NaCl}}$  is the osmotic efficiency calculated for a NaCl solution (mean  $\varepsilon$  and [range of  $\varepsilon$ ]). Elevation is in m NGF.

[36] Hydraulic head calculations, taking into account chemical osmosis with  $\varepsilon$  computed using the natural composition, result in closer simulation of the observed excess head profile. Indeed, fairly good agreement is observed between the calculated and measured heads, with a  $\sigma$  of 16%. The influence of the pore water composition on the calculated head profile is illustrated in Figure 7. Here the osmotically induced hydraulic heads calculated for a NaCl solution are 10–15 m higher than the value of 35 m calculated bearing in mind the natural pore water composition, and result in a  $\sigma$  of 29% compared with the measured heads. The measured excess head is better reproduced when the natural composition of the fluid is considered in the calculations, although both calculated head profiles are in the range of the measured profile.

[37] Uncertainty on the hydraulic head was evaluated from the experimental uncertainty of the petrophysical parameters (Table 1) used to calculate the intrinsic permeability and the chemo-osmotic efficiency. A maximum numerical uncertainty of  $\pm 1$  m on the heads occurs where the highest changes in mineralogy and petrology are observed in the formation, i.e., in the lower Toarcian.

[38] These calculations suggest that the measured excess head profile in the Toarcian/Domerian argillaceous formation of Tournemire can be explained by chemical osmosis and vertical permeability variations. However, this analysis of the excess head is partial because thermo-osmosis, a fluid flow driven by a temperature gradient, was also observed and quantified in the Tournemire argillite [Tremosa *et al.*, 2010] and is expected to have an influence on fluid flows and the hydraulic head profile in the formation.

[39] Regarding the fluid flow and mass transport, modifications induced by chemical osmosis are relatively limited compared with the case considering only hydraulic flow with variable permeability. Fluid flow remains directed downward in both cases. The Peclet number, which describes the relative importance of convection and diffusion, is 0.28 when only hydraulic flow is considered and 0.30 when chemo-osmotic and hydraulic flows are considered together. Thus, mass transport remains mainly governed by diffusion.

## 5. Conclusions

[40] The effect of natural water compositions compared to simple NaCl solutions, commonly used in experiments

and in theoretical calculations, on osmotic efficiency and abnormal pressures in natural clay rocks was evaluated. This evaluation was based on an electrical triple-layer model (TLM) developed to calculate the chemo-osmotic efficiency of compacted clay rocks characterized by complex pore fluid compositions. Compared to the osmotic overpressures of up to 1.6 MPa predicted considering purely NaCl solutions, lower overpressures are predicted when  $\text{Ca}^{2+}/\text{Na}^+$  mixed solutions are considered. Considering pore water solutions with both monovalent and divalent cations tends to decrease the extent of the diffuse layer in the pore space. Consequently, the osmotic efficiency of the shale also decreases and tends toward lower abnormal pressures. For a Na-Ca ratio of 18:1, the osmotic efficiency is predicted to be half of that of a pure  $\text{Na}^+$  solution, and the resulting overpressure is also half. However, the TLM was calibrated on osmotic efficiencies obtained during experiments using only NaCl as the test solution. Indeed, no chemo-osmotic experiments thus far have been performed on natural shales considering different test water compositions for a same salinity. As a result, the predicted osmotic efficiency of a shale for natural water compositions continues to be validated by experiments. Since natural waters are generally composed of species of various valences, lower osmotic efficiencies than those measured in most experiments using NaCl solutions can be expected in shale layers. Thus, a primary difference between predicted versus measured abnormal pressures therefore can be attributed to the more complex chemical compositions of actual sedimentary basins relative to those based on simplified laboratory experiments.

[41] Excess fluid pressures were calculated in sedimentary basins at steady state conditions for salinity. These conditions are not usually considered suitable for the occurrence of such overpressures. Indeed, osmotic overpressures are exclusively studied as a transient-state situation depending on the concentration difference between the center of the argillaceous layer with a high salinity and the surrounding aquifers. In spite of being moderate in magnitude (less than 0.1 MPa), overpressures can be generated assuming a linear concentration profile because of the chemo-osmotic efficiency coefficient dependence on the chemical concentration and composition and the half-pore size. However, such moderate osmotic overpressures can hardly be measured in shales.

[42] The case study of the Toarcian/Domerian argillaceous formation of Tournemire, showing moderate excess hydraulic heads of  $\sim 30$  m, was considered in support of the contentions noted in this study. The measured excess head was correctly reproduced when hydraulic and chemosmotic flows were considered together with the vertical variations in the hydraulic permeability and the chemosmotic efficiency calculated using the TLM. The results suggest that the variations in permeability and chemical osmosis explain the excess head profile measured at Tournemire. A noticeable difference of 10–15 m was observed between the calculated hydraulic heads for the natural pore water composition and for NaCl solution at the same ionic strength. A better agreement was thus obtained using the natural pore water composition to estimate the osmotic efficiency.

### Appendix A: Triple-Layer Model TLM Developed for Mixed Ca/Na Solutions

[43] The electrical triple-layer model (TLM) developed herein to describe the interactions between the charged solid surface of a clay rock and the pore solution represents an extension of the *Avena and De Pauli* [1998] double-layer model (DLM) and the *Leroy and Revil* [2004] TLM. This model was modified by *Gonçalvès et al.* [2007] to account for overlapping diffuse layers. Multicomponent solutions were introduced herein to this latter version following the approach by *Leroy et al.* [2007]. The advantage of the TLM compared to the DLM is the treatment of ions as particles of finite size, so that high-ionic concentrations near the surface can be considered [*Horseman et al.*, 1996]. Introducing the interaction of diffuse layers, by a truncation of these layers, is related to the small pore size in such rocks. As stated, osmotic phenomena result from this truncation. Multicomponent solutions with monovalent and divalent cations are introduced in the model enabling the exchange of various cations on surface sites.

[44] Geometrically, the TLM considers two compacted layers constituted of ions sorbed at the mineral surface, i.e., the Stern layer. These layers are limited by the inner Helmholtz plane (IHP) and outer Helmholtz plane (OHP). This last plane forms the limit of the Stern layer and the beginning of the diffuse layer, i.e., the third layer considered in the TLM starts at the OHP. The diffuse layer extends toward the pore center and is limited by the interaction with the diffuse layer of another clay mineral particle.

[45] A schematic description is depicted in Figure A1. TLM considers the surface sites linked to the permanent negative charge due to isomorphous substitution and the variable charge hydroxyl surface sites for protonation/deprotonation. Permanent exchange surface sites are represented here as  $X$  sites and each site carries one negative charge ( $X^-$ ). The exchange half-reactions for  $\text{Na}^+$ ,  $\text{Ca}^{2+}$ , and  $\text{H}^+$  with their respective reaction constants are as follows:

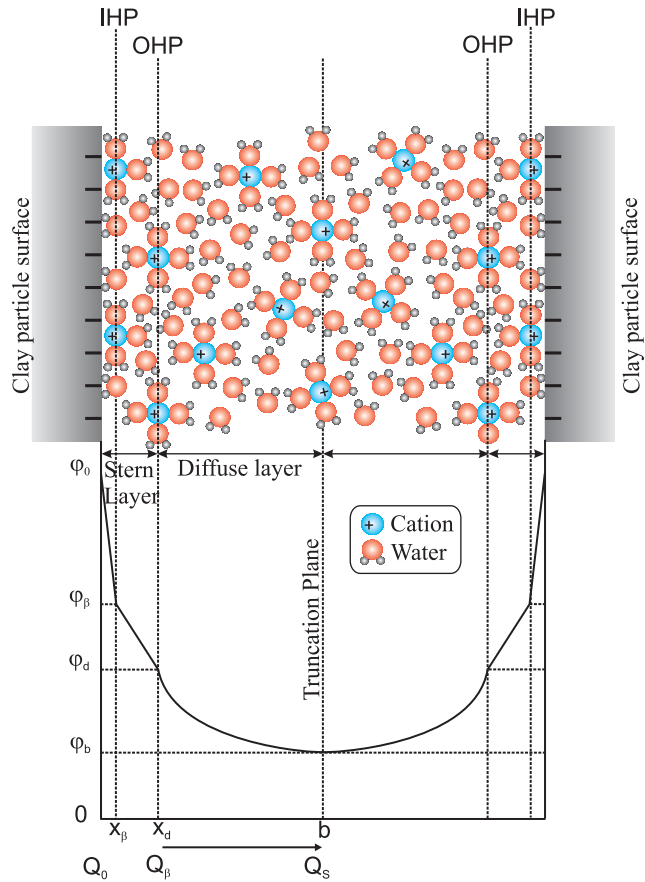
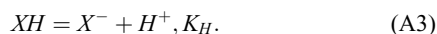
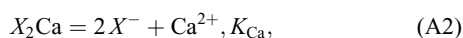


**Figure A1.** Schematic representation of solution–mineral surface interactions and associated electrochemical variables (electrical potentials  $\varphi_i$  and surface charges  $Q_i$ ) in the TLM with interacting diffuse layers [*Gonçalvès et al.*, 2010]. IHP: inner Helmholtz plane; OHP: outer Helmholtz plane.

The surface site density  $\Gamma_i^0$  (in sites  $\text{m}^{-2}$ ) for each species  $i$  is expressed from the reaction constant expressions, which in the *Gaines and Thomas* [1953] convention, can be written as follows:

$$\Gamma_{XH}^0 = \frac{\Gamma_{X^-}^0 a_{\text{H}^+}}{K_H}, \quad (\text{A4})$$

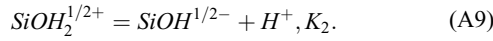
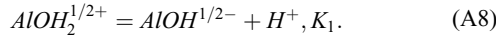
$$\Gamma_{X\text{Na}}^0 = \frac{\Gamma_{X^-}^0 a_{\text{Na}^+}}{K_{\text{Na}}}, \quad (\text{A5})$$

$$\Gamma_{X_2\text{Ca}}^0 = \frac{(\Gamma_{X^-}^0)^2 a_{\text{Ca}^{2+}}}{K_{\text{Ca}}}, \quad (\text{A6})$$

where  $a_i$  is the activity of species  $i$ . The  $\Gamma_{X^-}^0$  expression is obtained using the total surface site density of the  $X$  sites,  $\Gamma_3^0$ , by the Newton method:

$$\Gamma_3^0 = \Gamma_{X^-}^0 + \Gamma_{XH}^0 + \Gamma_{X\text{Na}}^0 + \Gamma_{X_2\text{Ca}}^0. \quad (\text{A7})$$

$\Gamma_1^0$  and  $\Gamma_2^0$  correspond to the total surface site density of aluminol and silanol hydroxyl sites, obtained from the following complexation reactions:



The surface charge density of the clay minerals  $Q_0$  ( $C\ m^{-2}$ ) is obtained, using surface site density, by the following equation:

$$Q_0 = -e \left[ \frac{1}{2} (\Gamma_{AlOH_2^{1/2+}}^0 - \Gamma_{AlOH^{1/2-}}^0 + \Gamma_{SiOH_2^{1/2+}}^0 - \Gamma_{SiOH^{1/2-}}^0) - \Gamma_3^0 \right], \quad (A10)$$

where  $e$  is the elementary charge ( $1.6 \times 10^{-19}$  C). The charge density in the Stern layer  $Q_\beta$  can be expressed as

$$Q_\beta = e(\Gamma_{XNa}^0 + 2\Gamma_{X_2Ca}^0 + \Gamma_{XH}^0). \quad (A11)$$

Potentials in the IHP and the OHP drop linearly and are related to the charge densities by the relationships:

$$\varphi_0 - \varphi_\beta = Q_0/C_1, \quad (A12)$$

$$\varphi_\beta - \varphi_d = Q_\beta/C_2, \quad (A13)$$

where  $\varphi_0$ ,  $\varphi_\beta$ , and  $\varphi_d$  are, respectively, the electrical potentials (V) at the surface, at the  $\beta$  plane (IHP), and the  $d$  plane (OHP).  $C_1$  and  $C_2$  are the capacities ( $F\ m^{-2}$ ) between the surface and the IHP and between the IHP and the OHP, respectively.

[46] In the diffuse layer, the electrical potential and the ionic concentrations are obtained by the Poisson-Boltzmann equation. The charge density in the diffuse layer  $Q_S$  is written as follows, for a solution with  $N$  species  $i$  and a distance from the mineral surface  $x_d$  to  $b$ , i.e., from the OHP to the truncation plane:

$$Q_S = \int_{x_d}^b \sum_{i=1}^N \frac{C_i^f \gamma_i^f}{\gamma_i} e z_i \exp\left(-\frac{z_i e \varphi}{k_B T}\right) dx, \quad (A14)$$

where  $k_B$  is the Boltzmann constant ( $1.38 \times 10^{-23}$  J K<sup>-1</sup>),  $T$  is the temperature (K),  $z_i$  is the valence of the ion  $i$ , and  $C_i^f$  is the concentration of species  $i$  in the equilibrium solution ( $mol\ L^{-1}$ ). This concentration,  $C_i^f$ , is the concentration in the porous media out of the electrostatic field influence denoted as the equilibrium solution and corresponds to the concentration obtained by a classical geochemical model.  $\gamma_i^f$  and  $\gamma_i$  are the activity coefficients, calculated with the Davies [1962] equation, in the equilibrium solution and in the diffuse layer, respectively. The Davies [1962] equation can be used for solutions with salinity lower than 0.7 M [Langmuir, 1997], i.e., up to seawater salinity.

[47] The last equation of the TLM is its global electroneutrality constraint:

$$Q_0 + Q_\beta + Q_S = 0. \quad (A15)$$

[48] The chemo-osmotic efficiency coefficient is obtained from the resolution of the Navier-Stokes equation integrating the chemical force [Bolt, 1979] for a porous medium with a plane-parallel geometry, or

$$\varepsilon = \frac{\int_0^b (1 - \frac{\overline{C^-}(x)}{C_f})(2bx - x^2) dx}{\frac{2b^3}{3}}, \quad (A16)$$

where  $\overline{C^-}(x)$  is the anion concentration at a distance  $x$  from the clay surface,  $C_f$  is the anion concentration in the equilibrium solution, and  $2b$  is the pore size. It is worth noting that anion exclusion expression is applicable for both symmetric and nonsymmetric solutions [Bolt, 1979].

[49] The predictions of the TLM for multi-ionic solutions with interacting diffuse layers were calibrated against osmotic efficiency data of various natural clay rocks in a NaCl-clay system [Neuzil, 2000; Cey et al., 2001; Al-Bazali, 2005; Garavito et al., 2006, 2007; Horseman et al., 2007; Rousseau-Gueutin et al., 2009, 2010]. Resulting parameters are  $\Gamma_1^0 = 0$  sites  $nm^{-2}$ ,  $\Gamma_2^0 = 0.52$  sites  $nm^{-2}$ ,  $\Gamma_3^0 = 2.58$  sites  $nm^{-2}$  (obtained with the cation exchange capacity [CEC] and the specific surface area),  $K_1$  undetermined,  $K_2 = 1.3 \times 10^{-6}$ ,  $K_H = 1 \times 10^{-2}$ ,  $K_{Na} = 1.3 \times 10^{-1}$ ,  $K_{Ca} = 5 \times 10^{-3}$  [Avena and De Pauli, 1998; Leroy and Revil, 2004; Gaucher et al., 2006; Gonçalves et al., 2007],  $C_1 = 1\ F\ m^{-2}$  and  $C_2 = 0.2\ F\ m^{-2}$ . As observed by Gonçalves et al. [2007], the more sensitive parameters are  $K_{Na}$  and  $C_2$ .

[50] **Acknowledgments.** This work was performed as part of J. Tremosa's Ph.D thesis, funded by IRSN (French Institute for Radiological protection and Nuclear Safety) and Amphos 21 Consulting S.L. J. Gonçalves acknowledges the CNRS (French National Center for Scientific Research) through the GNR FORPRO II. The constructive comments of the Ph.D examiners, P. Cosenza and P. Gouze, on this work are gratefully acknowledged. Our thanks also extend to two anonymous reviewers and C. E. Neuzil for notably improving this paper.

## References

- Al-Bazali, T. M. (2005), Experimental study of the membrane behavior of shale during interaction with water-based and oil-based muds, Ph.D. thesis, Univ. of Texas, Austin.
- Ambert, M., and P. Ambert (1995), Karstification des plateaux et encaissement des vallées au cours du Néogène et du Quaternaire dans les Grands Causses méridionaux (Larzac, Blandas), *Géologie de la France*, 4, 37–50.
- Avena, M. J., and C. P. De Pauli (1998), Proton adsorption and electrokinetics of an Argentinean montmorillonite, *J. Colloid Interface Sci.*, 202, 195–204.
- Bertrand, L., R. Lavignerie, J. Cabrera, J. M. Matray, and S. Savoye (2002), Instrument for measuring pore pressure and permeability in low permeability rock, paper presented at 1st International Meeting on Clays in Natural and Engineered Barriers for Radioactive Waste Confinement, December 9–12 2002, ANDRA, Reims, France.
- Boisson, J.-Y. (2005), Clay club catalogue of characteristics of argillaceous rocks, *Nuclear Energy Agency Rep. 4436*, Organisation for Economic Co-operation and Development OECD, Issy-les-Moulineaux, France.
- Boisson, J. Y., L. Bertrand, J. F. Heitz, and Y. Moreau Le Golvan (2001), In-situ and laboratory investigations of fluid flow through an argillaceous formation at different scales of space and time, Tournemire tunnel, southern France, *Hydrogeol. J.*, 9, 108–123.
- Bolt, G. H. (1979), *Soil Chemistry, B. Physicochemical Models*, 480 pp., Elsevier, Amsterdam, Netherlands.
- Bresler, E. (1973), Anion exclusion and coupling effects in nonsteady transport unsaturated soils: I. Theory, *Soil Sci. Soc. Am. Proc.*, 37(5), 663–669.

- Cey, B. D., S. L. Barbour, and M. J. Hendry (2001), Osmotic flow through a Cretaceous clay in southern Saskatchewan, Canada, *Can. Geotech. J.*, *38*(5), 1025–1033.
- Chilingar, G. V., V. A. Serebryakov, and J. O. J. Robertson (2002), *Origin and Prediction of Abnormal Formation Pressures*, Developments in Petroleum Science, vol. 50, 373 pp., Elsevier, Amsterdam, Netherlands.
- Davies, C. W. (1962), *Ion Association*, 190 pp., Butterworths, Washington, D. C.
- de Marsily, G. (1986), *Quantitative Hydrogeology, Groundwater Hydrology for Engineers*, 440 pp., Academic, N. Y.
- Fritz, S. J. (1986), Ideality of clay membranes in osmotic processes: A review, *Clays Clay Miner.*, *34*(2), 214–223.
- Gaines, G. I., and H. C. Thomas (1953), Adsorption studies on clay minerals. II. A formulation of the thermodynamics of exchange adsorption, *J. Phys. Chem.*, *21*, 714–718.
- Garavito, A. M., H. Kooi, and C. E. Neuzil (2006), Numerical modeling of a long-term in situ chemical osmosis experiment in the Pierre Shale, South Dakota, *Adv. Water Resour.*, *29*, 481–492.
- Garavito, A. M., I. De Cannière, and H. Kooi (2007), In situ chemical osmosis experiment in the Boom Clay at the Mol underground research laboratory, *Phys. Chem. Earth*, *32*, 421–433.
- Gaucher, E., et al. (2006), Modelling the porewater chemistry of the Callovo-Oxfordian formation at a regional scale, *Comptes Rendus Geoscience*, *338*, 917–930.
- Gonçalvès, J., S. Violette, and J. Wending (2004), Analytical and numerical solutions for alternative overpressuring processes: Application to the Callovo-Oxfordian sedimentary sequence in the Paris basin, France, *J. Geophys. Res.*, *109*, B02110, doi:10.1029/2002JB002278.
- Gonçalvès, J., P. Rousseau-Gueutin, and A. Revil (2007), Introducing interacting diffuse layers in TLM calculations. A reappraisal of the influence of the pore size on the swelling pressure and the osmotic efficiency of compacted bentonites, *J. Colloid Interface Sci.*, *316*, 92–99.
- Gonçalvès, J., P. Rousseau-Gueutin, G. de Marsily, P. Cosenza, and S. Violette (2010), What is the significance of pore pressure in a saturated shale layer?, *Water Resour. Res.*, *46*, W04514, doi:10.1029/2009WR008090.
- Hendry, M. J., and L. Wassenaar (1999), Implications of the distribution of  $^3\text{D}$  in porewaters of groundwater flow and the timing of geological events in a thick aquitard system, *Water Resour. Res.*, *35*(6), 1751–1760.
- Horseman, S. T., J. J. W. Higgo, J. Alexander, and J. F. Harrington (1996), Water, gas and solute movement through argillaceous media, Nuclear Energy Agency (NEA), a subgroup of the NEA Co-ordinating Group on Site Evaluation and Design of Experiments for Radioactive Waste Disposal (SEDE), *Rep. 96/1 OECD*, 290 pp., Paris, France.
- Horseman, S. T., J. F. Harrington, and D. J. Noy (2007), Swelling and osmotic flow in a potential host rock, *Phys. Chem. Earth*, *32*, 408–420.
- Kemper, W. D., and J. B. Rollins (1966), Osmotic efficiency coefficients across compacted clays, *Soil Sci. Soc. Am. Proc.*, *30*(5), 529–534.
- Langmuir, D. (1997), *Aqueous Environmental Geochemistry*, 600 pp., Prentice Hall, Upper Saddle River, N. J.
- Lee, Y., and D. Deming (2002), Overpressures in the Anadarko Basin, Southwestern Oklahoma: Static or dynamic?, *AAPG Bull.*, *86*, 145–160.
- Leroy, P., and A. Revil (2004), A triple-layer model of the surface electrochemical properties of clay minerals, *J. Colloid Interface Sci.*, *270*, 371–380.
- Leroy, P., A. Revil, S. Altmann, and C. Tournassat (2007), Modeling the composition of the pore water in a clay-rock geological formation (Callovo-Oxfordian, France), *Geochim. Cosmochim. Acta*, *71*, 1087–1097, doi:10.1016/j.gca.2006.11.009.
- Magara, K. (1980), Comparison of porosity-depth relationships of shale and sandstone, *J. Pet. Geol.*, *3*, 175–185.
- Marine, I. W., and S. J. Fritz (1981), Osmotic model to explain anomalous hydraulic heads, *Water Resour. Res.*, *17*(1), 73–82.
- Matray, J. M., S. Savoye, and J. Cabrera (2007), Desaturation and structure relationships around drifts excavated in the well-compacted Tournemire's argillite (Aveyron, France), *Eng. Geol.*, *9*, 1–16.
- Mazurek, M., et al. (2011), Natural tracer profiles across argillaceous formations, *Appl. Geochem.*, *26*, 1035–1064.
- Mitchell, J. K., and K. Soga (2005), *Fundamentals of Soil Behavior*, 3rd ed., 558 pp., John Wiley, N. Y.
- Neuzil, C. E. (1994), How permeable are clays and shales?, *Water Resour. Res.*, *30*(2), 145–150, doi:10.1029/93WR02930.
- Neuzil, C. E. (1995), Abnormal pressures as hydrodynamic phenomena, *Am. J. Sci.*, *295*, 742–786.
- Neuzil, C. E. (2000), Osmotic generation of “anomalous” fluid pressures in geological environments, *Nature*, *403*, 182–184.
- Neuzil, C. E. (2003), Hydromechanical coupling in geologic processes, *Hydrogeol. J.*, *11*, 41–83.
- Neuzil, C. E., and A. M. Provost (2009), Recent experimental data may point to a greater role for osmotic pressures in the subsurface, *Water Resour. Res.*, *45*, W03410, doi:10.1029/2007WR006450.
- Patriarche, D., E. Ledoux, J.-L. Michelot, R. Simon-Coinçon, and S. Savoye (2004), Diffusion as the main process for mass transport in very low water content argillites: 2. Fluid flow and mass transport modeling, *Water Resour. Res.*, *40*, W01517, doi:10.1029/2003WR002700.
- Pearson, F. J., et al. (2003), Geochemistry of water in the Opalinus clay formation at the Mont Terri rock laboratory, *Technical Rep. 2003-03*, Mont Terri Project, Swiss Federal Office for Water and Geology, Bern, Germany.
- Peyaud, J. B., J. Barbarand, A. Carter, and M. Pagel (2005), Mid-Cretaceous uplift and erosion on the northern margin of the Ligurian Tethys deduced from thermal history reconstruction, *Int. J. Earth Sci.*, *94*, 46247.
- Revil, A., and P. Leroy (2004), Constitutive equations for ionic transport in porous shales, *J. Geophys. Res.*, *109*, B03208, doi:10.1029/2003JB002755.
- Rousseau-Gueutin, P., V. de Greef, J. Gonçalvès, S. Violette, and S. Chanchole (2009), Experimental device for chemical osmosis measurement on natural clay-rock samples maintained at in-situ conditions. Implications for pressure interpretation, *J. Colloid Interface Sci.*, *337*, 106–116.
- Rousseau-Gueutin, P., J. Gonçalvès, M. Cruchaudet, G. de Marsily, and S. Violette (2010), Hydraulic and chemical pulse-tests in a shut-in chamber imbedded in an argillaceous formation: Numerical and experimental approaches, *Water Resour. Res.*, *46*, W08516, doi:10.1029/2008WR007371.
- Shackelford, C. D., and J. M. Lee (2003), The destructive role of diffusion on clay membrane behavior, *Clays Clay Miner.*, *51*, 186–196.
- Simon-Coinçon, R., and J. M. Schmitt (1999), Evolution géologique et histoire paléoenvironnementale du bassin des grands causses, *Rapport technique LHM/RD/99/52*, Centre d'Information Géologique, Ecole Nationale Supérieure des Mines de Paris, France.
- Swarbrick, R., and M. Osborne (1998), Mechanisms that generate abnormal pressures: an overview, in *Abnormal Pressures in Hydrocarbon Environments*, edited by B. E. Law et al., pp. 13–34, AAPG Memoir 70, Golden, Colo.
- Tremosa, J. (2010), Influence of osmotic processes on the excess-hydraulic head measured in the Toarcian/Domerian argillaceous formation of Tournemire, Ph.D. thesis, Université Pierre et Marie Curie, Paris 6, France.
- Tremosa, J., J. Gonçalvès, J. M. Matray, and S. Violette (2010), Estimating thermo-osmotic coefficients in clay-rocks: II. In situ experimental approach, *J. Colloid Interface Sci.*, *342*, 175–184.
- Tremosa, J., D. Arcos, J. M. Matray, F. Bensenouci, E. C. Gaucher, C. Tournassat, and J. Hadi (2012), Geochemical characterization and modelling of the Toarcian/Domerian porewater at the Tournemire underground research laboratory, *Appl. Geochem.*, doi:10.1016/j.apgeochem.2012.01.005, in press.
- Vinsot, A., S. Mettler, and S. Wechner (2008), In situ characterization of the Callovo-Oxfordian pore water composition, *Phys. Chem. Earth*, *33*, S75–S86.
- Walsh, J. B., and W. F. Brace (1984), The effect of pressure on porosity and the transport properties of rocks, *J. Geophys. Res.*, *89*, 9425–9431.
- Young, A., and P. Low (1965), Osmosis in argillaceous rocks, *AAPG Bull.*, *49*, 1004–1008.

J. Gonçalvès, CNRS, CEREGE, UMR-6635, Aix-Marseille University, Europôle Méditerranéen de l'Arbois, POB 80, Aix en Provence Cedex 4, 13545, France.

J.-M. Matray and J. Tremosa, IRSN, DEI/SARG/LR2S, BP 17, F-92262 Fontenay-aux-Roses, France. (j.tremosa@brgm.fr)

J. Tremosa, UMR-7619 SISYPHE, UPMC University of Paris 06, 4 place Jussieu, F-75252 Paris, France.